Highly Polarization-Sensitive, Broadband, Self-Powered Photodetector Based on Graphene/$PdSe_2$/Germanium Heterojunction

Di Wu,[†] Jiawen Guo,[†] Juan Du,[‡] Congxin Xia,[‡] Longhui Zeng,[, §] Yongzhi Tian,[†] Zhifeng Shi,[†] Yongtao Tian,[†] Xin Jian Li,[†] Yuen Hong Tsang,[*, §] and Jiansheng Jie[*, ‖]*

[†]School of Physics and Engineering, and Key Laboratory of Material Physics, Ministry of Education, Zhengzhou University, Zhengzhou, Henan 450052, China

[‡]College of Physics and Materials Science, Henan Normal University, Xinxiang, Henan 453007, China

[§]Department of Applied Physics and Materials Research Center, The Hong Kong Polytechnic University, Hung Hom, Kowloon, Hong Kong, China

[‖]Institute of Functional Nano & Soft Materials (FUNSOM), Soochow University, Suzhou, Jiangsu 215123, China

ABSTRACT: Polarization-sensitive photodetection in a broad spectrum range is highly desired due to the great significance in military and civilian applications. Palladium diselenide ($PdSe_2$), a newly explored air-stable, group-10 two-dimensional (2D) noble metal dichalcogenide with a puckered pentagonal structure, holds promise for polarization-sensitive photodetection. Herein, we report a highly polarization-sensitive, broadband, self-powered photodetector based on graphene/$PdSe_2$/germanium heterojunction. Owing to the enhanced light absorption of the mixed-dimensional van der Waals heterojunction and the effective carrier collection with graphene transparent electrode, the photodetector exhibits superior device performance in terms of a large photoresponsivity, a high specific detectivity, a fast response speed to follow nanosecond pulsed light signal and a broadband photosensitivity ranging from deep ultraviolet (DUV) to mid-infrared (MIR). Significantly, highly polarization-sensitive broadband photodetection with an ultrahigh polarization sensitivity of 112.2 is achieved, which represents the best result for 2D layered material-based photodetectors. Further, we demonstrated the high-resolution polarization imaging based on the heterojunction device. This work reveals the great potential of 2D $PdSe_2$ for high-performance, air-stable, and polarization-sensitive broadband photodetectors.

KEYWORDS: *$PdSe_2$, two-dimensional materials, polarization-sensitive photodetector, broadband photodetection, heterojunction*

In recent years, polarization-sensitive photodetectors have stimulated increasing research interests, due to their important applications in navigation, optical switch, and high-contrast polarizer.[1,2] To achieve high polarization sensitivity, it is much desired that the semiconductor has a strongly anisotropic photoresponse to polarized light.[3] Among different semiconductors for polarization-sensitive photodetection, two-dimensional (2D) layered materials such as black phosphorus (BP),[4] GeS_2,[5] silicene,[6] germanene,[7] and antimonene[8] have attracted particular attention, because of their anisotropic properties originated from asymmetric crystal structures, in which the buckling breaks the sublattice symmetry, enhances spin-orbit coupling, and allows tuning of a topological quantum phase transition.[9] For instance, a plasmonic resonance enhanced BP photodetector showed a polarization-sensitive photoresponse to infrared light with a polarization sensitivity of 8.7,[10] and a higher polarization sensitivity of ~22 was obtained for BP/MoS_2 heterojunction photodiode.[11] Also, a polarization-sensitive ultraviolet photodetector based on 2D GeS_2 film with a polarization sensitivity of 2.1 was reported.[5] In spite of the large progress, the poor air-stability and/or the wide bandgap of these 2D layered materials impede their wide application in stable, broadband polarization-sensitive photodetectors.

Palladium diselenide ($PdSe_2$) is an emerging high mobility 2D transition metal dichalcogenides (TMDs) with an indirect bandgap of ~1.3 eV for single layer and down to zero in the bulk form.[12] Such a narrow bandgap covering a broadband spectral range from deep ultraviolet (DUV) to mid-infrared (MIR) makes $PdSe_2$ a promising candidate for broadband detection applications. Recently, a broadband photodetector with a high responsivity (R) of 185.6 mA/W has been achieved for 2D $PdSe_2$/MoS_2 heterojunction. This device demonstrated an excellent air-stability over three months due to the high stability of $PdSe_2$.[13] Besides, to overcome the limitation of optical absorption for atomically thin 2D semiconductors, a $PdSe_2$/Si

2D/three-dimensional (3D) mixed-dimensional heterojunction photodetector was constructed, which exhibited a good device performance with a responsivity up to 300 mA/W and a specific detectivity (D^*) of 1.18×10^{13} Jones,[12] though the spectral sensitivity of the detectors was restricted to be <1100 nm due to the intrinsic bandgap of Si (~1.1 eV). Interestingly, similar to BP and silicene, 2D $PdSe_2$ film also possesses an asymmetric crystal structure with a puckered pentagonal arrangement. It has been demonstrated that the $PdSe_2$ film has exotic anisotropic properties due to its low-symmetry crystal structure.[3] However, polarization-sensitive broadband photodetectors based on 2D layered $PdSe_2$ film is yet to be reported.

Herein, we demonstrate the construction of a highly polarization-sensitive, broadband, self-powered photodetector based on graphene (Gr)/$PdSe_2$/germanium (Ge) heterojunction. This strategy has several important advantages: (i) Compared to Si, Ge has a larger absorption coefficient and a narrower bandgap of ~0.67 eV, enabling the further extension of the wavelength detection range of the heterojunction. Also, the use of a graphene transparent electrode allows the effective light absorption and also enhances the carrier collection efficiency. (ii) Owing to the high-quality 2D/3D mix-dimensional van der Waals heterojunction, photodetector based on the heterojunction exhibits an excellent device performance with a large photoresponsivity, a high specific detectivity, a fast response speed and a broadband photosensitivity ranging from DUV to MIR. (iii) Significantly, polarization sensitivity as high as 112.2 is achieved for the Gr/$PdSe_2$/Ge heterojunction photodetector, which represents the best result for the 2D layered material-based polarization-sensitive photodetectors. High-resolution polarization imaging is further demonstrated based on the heterojunction photodetector. It is expected that the Gr/$PdSe_2$/Ge heterojunction will have important application in air-stable, broadband and polarization-sensitive photodetection.

RESULTS AND DISCUSSIONS

As illustrated in Figure 1a, 2D layered $PdSe_2$ has a pentagonal manner and can crystallize into an orthorhombic structure (*Pbca* space group) with the three atomic layers stacking in the order of Se-Pd-Se by weak van der Waals forces.[14] In this work, the $PdSe_2$ films were synthesized through one step of direct selenization of pre-deposited Pd layer.[11] X-ray diffraction (XRD) pattern in Figure S1a reveals the diffraction peaks at 22.9°, 32.9° and 61.5°, corresponding to (002), (021) and (133) planes of $PdSe_2$, respectively. No extra Pd peaks are observed in the pattern, suggesting that the pre-deposited Pd layer has been fully transformed into $PdSe_2$ with a high phase purity. It is noteworthy that wafer-scale $PdSe_2$ film could be successfully fabricated on a 2-inch SiO_2/Si substrate through the simple selenization method (Figure S1b); the color evolution from dark khaki to dark blue has demonstrated the transformation of Pd layer to $PdSe_2$ film. Raman spectra of the as-synthesized $PdSe_2$ film consist of four distinct peaks at 143.2, 205.5, 221.3, and 256.6 cm^{-1} (Figure S2a), which could be assigned to A^1_g, A^2_g, B_{1g}, and A^3_g vibration modes of $PdSe_2$, respectively. The peaks of A^1_g, A^2_g, and B_{1g} mainly involve the vibrations of Se, while the strongest mode of A^3_g is correlated to the relative vibration between Se and Pd atoms.[14] Raman spectra acquired from five different points on a 2-inch sample show excellent consistency. In addition, 2D Raman mapping over a relatively large area of 20×20 μm^2 was performed (Figure S2b). The uniform peak intensity distribution obtained from a series of Raman spectra is clearly observed, indicating the high homogeneity and uniformity of as-synthesized $PdSe_2$ film.

In view of the anisotropic properties of 2D $PdSe_2$, the polarization-dependent Raman spectra of $PdSe_2$ film were measured, as shown in Figure 1b. The polarization angle of 0° is defined as the *x*-axis, as labeled in Figure 1a. It can be found that the intensities of A^1_g and A^3_g modes

decrease when the polarization angle increases from 0° to 90°, and then increase again when the polarization angle changes from 90° to 180°. The polarization angle-dependent intensities for Raman peaks of A^1_g and A^3_g are plotted in Figure S3, suggesting that the Raman spectra of $PdSe_2$ film is polarization-dependent. Furthermore, theoretical calculations were conducted to study the optical absorbance of $PdSe_2$ film along *x*, *y* and *z* axes, respectively (Figure 1c). It is observed that the $PdSe_2$ film possesses distinct optical absorption properties along different directions in a broad wavelength range. The above results experimentally and theoretically confirm the optical anisotropy of $PdSe_2$ film, indicating the polarization-sensitive nature of 2D $PdSe_2$ film. Cross-sectional high-resolution transmission electron microscopy (HRTEM) image, Figure 1d, reveals that the as-synthesized $PdSe_2$ films is multilayer (~53 layers) with a thickness of ~22.8 nm along [002] orientation, which is in good agreement with the atomic force microscopy (AFM) measurement (Figure 1e). We noted that the selenization method allows the fabrication of $PdSe_2$ films with thickness down to ~4 monolayers (Figure S4). Further, from the X-ray photoelectron spectroscopy (XPS) results in Figure 1f, well-defined double peaks are presented for the film, suggesting the presence of Pd^{4+} and Se^{2-} with a ratio of ~ 1:2.06 in the film.

Figure 2a displays a schematic diagram the Gr/$PdSe_2$/Ge heterojunction photodetector, and the photograph of the real device is shown in the inset of Figure 2b. The device was fabricated by directly transferring 2D $PdSe_2$ film onto a Ge wafer with a pre-defined SiO_2 window. We note that the transfer process will not affect the integrality of $PdSe_2$ film (Figure S5). Graphene and In-Ga alloy were then adopted as transparent electrode for $PdSe_2$ film and ohmic contact for Ge substrate, respectively (Figure S6). Figure 2b plots the typical current-voltage (*I-V*) curve of the heterojunction measured in the dark. Notably, the device displays an obvious rectifying behavior with a forward-to-reverse bias current ratio as high as ~2.4×10^3, which has surpassed those of

other heterojunction devices, such as Gr/Ge (~50),[15] $PtSe_2$/Si (~100)[16] and $PdSe_2/MoS_2$ (~30)[13] heterojunctions. In addition, the ideality factor (n) of the Gr/$PdSe_2$/Ge heterojunction can be deduced from the following equation:

$$n = \frac{q}{k_B T} \frac{dV}{d \ln I} \quad (1)$$

where I_0, q, n, k_B and T are reverse leakage current, unit charge, ideality factor, Boltzmann's constant and Kelvin temperature, respectively. Hence, n can be calculated to be 1 at a low voltage zone (0-0.3 V), which is in good agreement with the theoretical value (n = 1).[17] The small ideality factor, along with the excellent rectifying characteristic, confirms the high quality of the $PdSe_2$/Ge junction.

Next, we measured the photoresponse characteristics of the Gr/$PdSe_2$/Ge heterojunction device. As shown in Figure 2c, when the device is illuminated by light signals, the current of the heterojunction at reverse bias direction increases dramatically. The current at bias voltage of -5 V increases from 4.3×10^{-5} A in dark to 1.6×10^{-4} A at 265 nm (1.7 mW/cm^2), 7.6×10^{-4} A at 3043 nm (600 mW/cm^2), 2×10^{-3} A at 1550 nm (11.5 mW/cm^2), 1.8×10^{-2} A at 780 nm (51.5 mW/cm^2) and 2.4×10^{-2} A at 980 nm (61.3 mW/cm^2). Close observation of the enlarged curves under different wavelengths reveals the obvious photovoltaic effect of the device (Figure S7). The broadband photoresponse and photovoltaic property of this heterojunction device make it suitable to serve as a self-powered broadband photodetector. Figure 2d depicts time-resolved photoresponse of the device to light signals with different wavelengths under zero bias. We note that the device is stable and has fast responses to incident lights with wavelength ranging from DUV (265 nm) to MIR (3043 nm). Note that photodetectors with a superior detection capability covering multiband spectral range are pivotal importance for the applications in night vision, military warning, imaging sensor, and optical communication.[18]

To quantitatively evaluate photoresponse performance of the Gr/$PdSe_2$/Ge heterojunction device, the key device parameters of a photodetector, *i.e.* responsivity (R) and specific detectivity (D*), can be calculated based on the following formulas:[19]

$$R = \frac{I_{Ph} - I_D}{P_{opt} \cdot S} \tag{2}$$

$$D^* = \frac{\sqrt{AB}}{\sqrt{\overline{i_n^2}}} R \tag{3}$$

where I_D, P_{opt}, S, A , B and $\sqrt{\overline{i_n^2}}$ are the dark current, light intensity, illumination area, device area, bandwidth and the mean-square noise current measured at the bandwidth of 1 Hz in darkness (Figure S8), respectively. Figure 2e shows the wavelength-dependent R and D* of the device measured under the same light intensity. Significantly, the heterojunction device exhibits a broadband spectral response covering of 200-2200 nm. It is observed that the device has a peak photoresponse from 600 to 1850 nm, which is well consistent with the UV-Vis-IR absorption spectrum of $PdSe_2$/Ge hybrid system (Figure 2f). For comparison, the absorption spectra of both $PdSe_2$ and planar Ge were measured. Apparently, the combination of $PdSe_2$ film and Ge substrate can effectively enhance the light absorption of the hybrid system.

The device performance was further investigated under the irradiation of 980 nm light with varied light intensity. Figure 3a and b depict a series of light intensity-dependent I-V curves of the heterojunction device. One can see that the reverse current increases with increasing light intensity. A short-circuit current (I_{sc}) of 0.48 mA and an open-circuit voltage (V_{oc}) of 0.11 V can be obtained for the device under a light intensity of 60.3 mW/cm^2 (Figure 3b). Besides, the time-resolved photoresponse of the device under a pulsed 980 nm light irradiation with different light intensities was investigated at a self-powered mode, as shown in Figure 3c. Apparently, the

$PdSe_2$-based heterojunction photodetector can be fast switched on/off with excellent stability and reproducibility, yielding a highest current on/off ratio (I_{on}/I_{off}) of 3×10^5 under a light intensity of 60.3 mW/cm^2. The I_{on}/I_{off} could be 22 even under a weak light intensity of 2.8 μW/cm^2. Moreover, the device can work well after 5000 cycles operation (Figure 3d), and can keep its initial infrared response properties even after storing in air for 6 months (Figure S9). The excellent stability of Gr/$PdSe_2$/Ge heterojunction photodetector could be attributed to the following aspects: (i) the excellent air stability of $PdSe_2$ film. From Figure S10, the XPS and Raman spectra of the $PdSe_2$ film are virtually unchanged after six months storage in air. (ii) the vertically stacked heterojunction structure. The top graphene and $PdSe_2$ layers can protect the underlying Ge substrate from the surface oxidation. Furthermore, the dependence of photocurrent on light intensity can be fitted well by the power law of $I_{ph} \propto P^{\theta}$, giving rise to a θ value of 0.87. This value is close to that for an ideal photodetector (θ = 1), verifying the high quality of the $PdSe_2$/Ge heterojunction.[20] Figure 3f shows the light intensity-dependent R and D^* values for the device measured under 980 nm light irradiation. Notably, the R value could reach 691 mA/W under a light intensity of 0.36 μW/cm^2 at zero bias, which is higher than that of the $PtSe_2$-based detectors (262-490 mA/W),[16,21,22] and has surpassed recently reported $PdSe_2$/Si (~300 mA/W)[12] and $PdSe_2$/MoS_2 (185.6 mA/W)[13] heterojunction photodetectors. Correspondingly, a highest D^* of 1.73×10^{13} Jones could be obtained for the device, which is also superior to previously reported devices (Table 1). These results collectively demonstrate that a high-performance, air-stable photodetector has been achieved based on the Gr/$PdSe_2$/Ge heterojunction.

Owing to the broadband light absorption of Gr/$PdSe_2$/Ge heterojunction, the device demonstrates an excellent photoresponse switching behavior in a wide spectrum range (Figure

4a-e). The device can follow the pulsed light of DUV (265 nm), optical communication and fiber optic cable testing band (1310 and 1550 nm), and MIR (3043 nm) with sharp photocurrent rise and fall edges. In addition, photocurrent of the device at the near-infrared (NIR) rang can be effectively tuning by controlling the light intensity; a large photocurrent of 0.22 mA is achieved for 1310/1550 nm light under a light intensity of 11.5 mW/cm^2, producing a high I_{on}/I_{off} ratio of 10^5. Also, the light intensity-dependent photocurrent can be fitted by the power law with power exponents of 0.95 and 0.98 for 1310 and 1550 nm lights, respectively. From Figure 4e, it is observed that the present device exhibits pronounce photoresponse to MIR light illumination (3043 nm) with a high I_{on}/I_{off} ratio over 5×10^2, which can be ascribed to the strong light absorption of $PdSe_2$/Ge hybrid system in MIR region. The photoresponse characteristics of Gr/$PdSe_2$/Ge heterojunction device can be further understood by the energy band diagram, as shown in Figure 4f. According to the theoretical calculations (Figure S11a and b), the bandgap of $PdSe_2$ film will decrease from 1.38 eV (monolayer) to 0 eV (bulk) with increasing the layer number, manifesting a transformation of the $PdSe_2$ film from semiconductor to semimetal. Also, we detected the work function (5.21 eV) of the multilayer $PdSe_2$ films in this work by using ultraviolet photoemission spectroscopy (UPS) (Figure S11c and d), confirming a nearly zero bandgap of the as-synthesized $PdSe_2$ film. Therefore, when the $PdSe_2$ film contacts with planar Ge, a built-in potential at the depletion region will be formed due to their difference in Fermi levels. For the light with photon energy larger than the bandgap of Ge, both the $PdSe_2$ film and Ge substrate will absorb the light. The photogenerated excitons will diffuse to the junction interface and then be separated by the built-in potential. Electrons will drift into the Ge substrate and then are collected by the graphene electrode, while holes will drift into the $PdSe_2$ film, forming the photocurrent. However, for the light with photon energy lower than the bandgap of

Ge (wavelength >1900 nm), the light is mainly absorbed by the $PdSe_2$ film. Electrons in $PdSe_2$ film can gain the energy from the photons to overcome the contact barrier at the junction interface, enabling the device to detect the NIR and MIR lights with wavelength up to 3043 nm.

As a key figure of merit, response speed of a photodetector reflects its ability to monitor the fast varied optical signals. Hence, the photoresponse of the Gr/$PdSe_2$/Ge heterojunction photodetector to pulsed light signals with different frequencies was investigated. A 980 nm laser driven by a signal generator with different frequencies was used to produce pulsed light signals, and the output photocurrent was recorded by an oscilloscope. Figure 5a depicts the representative photoresponse of heterojunction device to pulsed light signals with frequencies of 0.1, 1, 10 kHz, respectively. The device shows fast, stable and reversible photoresponse to varied optical signals but experiences an apparent degradation under a higher frequency (*e.g.* 10 kHz). From the relative balance $[(I_{max}-I_{min})/I_{max}]$ in Figure 5b, a high 3dB frequency (f_{3dB}) of 8 kHz are deduced, suggesting that the Gr/$PdSe_2$/Ge heterojunction photodetector is capable of detecting ultrafast optical signals. The response speed can be further evaluated by analyzing the rising and falling edges of an individual response cycle, which are defined as the time intervals for the response to rise from 10% to 90% and decay from 90% to 10% of its peak value.[23,24] Evident from Figure 5c, a rise/fall time of 6.4/92.5 μs is achieved from an enlarged response cycle at 5 kHz. We note that the response speed is comparable or even faster than other 2D TMD-based photodetectors.[25-28] The response speeds at different switching frequencies were plotted in Figure 5d, revealing the great potential of the photodetector to monitor ultrafast optical signals. To further evaluate the response of Gr/$PdSe_2$/Si heterojunction photodetector to an ultrafast pulse signal, the response characteristic of the device to a pulsed laser (266 nm, pulse width 1 ns, 1 kHz) was studied, as shown in Figure 5e and f. From the photoresponse switching curve, one can see that the

photodetector could accurately distinguish and response to each pulsed signal, giving rise to an ultrafast rise time of 112 ns for the rising edge. The fast response speed of Gr/$PdSe_2$/Si heterojunction photodetector is believed to be related to the quick separation and transportation of photo-generated electron-hole pairs by the built-in electric field at the junction interface. In addition, the vertically stacked heterojunction structure is beneficial to shorten the transmit time of the carriers, also contributing to a fast response speed. It is expected that the response speed could be further enhanced by the methods of reducing the effective device area, using Ge substrate with thinner thickness and so on.

As we known, to achieve high-precision detection of optical signals in complex environments, more information of the incident optical signal, such as the polarimetric information, is desirable to be obtained.[25] The 2D $PdSe_2$ film with an anisotropic crystal structure makes it highly sensitive to polarized light signal. In view of this, the polarization-dependent photoresponse of the Gr/$PdSe_2$/Ge heterojunction photodetector was explored. As shown in Figure S12, a polarizer, which can turn an incident light into a polarized light with controllable polarization angle, was placed between the light source and the photodetector. Figure 6a described the polarization-dependent current mapping of this heterojunction photodetector at revers bias from -5 V to 0 V under the light illumination of 650 nm. Significantly, it is observed that the measured photocurrent is highly dependent on the polarization angle as well as bias voltage. The photocurrent can reach a maximum value at a polarization angle of 0° (180°), while a minimum value is achieved at a polarization angle of 90° (270°) under each bias voltage. This result is in good agreement with the sine function. Meanwhile, it is found that the highest polarization sensitivity, defined as the photocurrent measured at a polarization angle of 0° divided by the photocurrent measured at 90°, is obtained at zero bias. Figure 6b plots the polarization angle-

dependent normalized photocurrent curves at zero bias under different wavelengths of 365, 650, 980 and 1550 nm. The polarization sensitivities are calculated to be 73.8 at 365 nm (40.5 mW/cm^2), 112.2 at 650 nm (52.6 mW/cm^2), 91.2 at 980 nm (60.3 mW/cm^2), and 53.8 at 1550 nm (11.5 mW/cm^2) under zero bias, revealing a broadband polarization sensitive nature of the 2D $PdSe_2$ film. Notably, the polarization sensitivity is much superior to previous reports on GeS_2 (2.1),[5] GeSe (2.16),[29] black phosphorus/MoS_2 heterojunction (22),[11] antimonene (17),[8] perovskite nanowire (~1.3),[30] GeO_2-Ge nanowire (4.2)[31] and so on. The polarization sensitivity of 112.2 at 650 nm for the polarization photoresponse also represents the highest value for 2D materials-based photodetectors reported so far. The excellent polarization-dependent photodetection performance of the Gr/$PdSe_2$/Ge heterojunction could be attributed to the following aspects: (i) the high-quality of as-synthesized large-area 2D $PdSe_2$ film with strong asymmetry;[32] (ii) the polarization response enhancement by the heterojunction structure compared with the $PdSe_2$ film (Figure S13). The built-in perpendicular electric field in the vertical heterojunction can serve to spatially separate the photogenerated carriers, and reduce the recombination probability for electrons and holes during their transportation;[4] (iii) the enhancement of the carriers collection efficiency by the graphene transparent electrode, which can also effectively suppress the carriers recombination at the junction interface.[26]

To exploit the potential applications of the Gr/$PdSe_2$/Ge heterojunction photodetector, infrared imaging ability of the Gr/$PdSe_2$/Ge heterojunction photodetector was further investigated. Figure 6c and Figure S14 display the schematic illustration for the measurement setup and digital photograph of the measurement system, respectively. A metal mask with hollow English letter of "P" controlled by a 2D motorized stage was put between the polarizer and the device. The polarized light passed through the mask and shined on the heterojunction device. With the

movement of the mask, the position-dependent voltage (or current) of the heterojunction device could be recorded in real time by a lock-in amplifier, which was further transformed into a voltage (or current) mapping image. Figure 6d shows the polarization-dependent infrared images measured under 780 nm illumination with polarization angles of 0° and 90°, respectively. A high-resolution image of "P" letter with a high voltage contrast ratio up to 3.25×10^3 is captured at a polarization angle of 0° (left of Figure 6d), while an image with a smaller voltage contrast ratio of 2.9×10^2 is obtained at a polarization angle of 90° (right of Figure 6d). Hence, a polarization contrast ratio over 10 is achieved, revealing the superior polarized light imaging capability of the heterojunction device. Moreover, MIR imaging based on the Gr/$PdSe_2$/Ge heterojunction photodetector is achieved. As shown in Figure 6e, an image of English letter of "Z" with a high current contrast ratio over 10^2 could be clearly recognized under 3043 nm light illumination. These results unambiguously demonstrate the great potential of Gr/$PdSe_2$/Ge heterojunction for polarization-sensitive broadband photodetection and imaging.

CONCLUSION

In summary, we demonstrated the fabrication of Gr/$PdSe_2$/Ge heterojunctions by directly transferring 2D $PdSe_2$ film onto a pre-patterned Ge wafer. Owing to the use of high-quality $PdSe_2$ film fabricated by a simple selenization approach, enhanced light harvesting by the mixed-dimensional van der Waals heterojunction, and improved carrier collection efficiency with graphene transparent electrode, the as-fabricated heterojunction exhibited an excellent device performance in terms of a large photoresponsivity of 691.5 mA/W, a high specific detectivity up to 1.73×10^{13} Jones, a fast response speed to follow nanosecond pulsed light signal, and an ultra-broadband photosensitivity ranging from DUV to MIR (200-3043 nm). Moreover, the device was demonstrated to be highly sensitive to polarized light in a broad spectrum range, giving rise to a

record high polarization sensitivity of 112.2 at 650 nm. High-resolution polarization imaging and MIR imaging capabilities were further demonstrated. Given the high stability and ultrahigh polarization sensitivity, the Gr/$PdSe_2$/Ge heterojunction devices holds promise for high-performance, polarization-sensitive broadband photodetection.

METHODS

Materials Synthesis and Characterization. The 2D layered $PdSe_2$ films were synthesized by a simple selenization approach, which has been described in detail in our previous work.[12] In this work, ~7 nm Pd film was deposited by magnetron sputtering for the synthesis of $PdSe_2$ film with a thickness of ~22.8 nm (Figure S15). In addition, high-quality few-layer graphene was prepared on 25 μm-thick copper foil *via* a chemical vapor deposition (CVD) method. Crystal structure and thickness of the $PdSe_2$ film were characterized by XRD (RigakuSmartLab) and AFM (VeecoNanoscope V), respectively. XPS measurements were carried out to detect the components of the film by using a monochromatic Al Kα source (1486.6 eV) provided by the XPS system (Thermo ESCALAB 250). Raman spectra were recorded on a Raman spectrometer equipped with 488 nm laser as an excitation source (Horiba HR800). The HRTEM analysis of the $PdSe_2$ film was performed by using a field-emission TEM (JEOL JEM-2100F).

Device Fabrication and Characterizations. To construct the Gr/$PdSe_2$/Ge heterojunction, a well-defined SiO_2 layer (100 nm) with a hollowed square window (0.5×0.5 cm^2) was deposited on an *n*-type Ge wafer (1-5 Ω·cm) using a shadow mask *via* magnetron sputtering. Afterward, the PMMA-supported $PdSe_2$ film was directly transferred onto the pre-patterned Ge wafer through a typical wetting-transferred method.[33] After removing the PMMA layer in acetone, a few-layer graphene film was transferred onto the top of the heterojunction as transparent electrode. Au (50 nm) deposited by magnetron sputtering served as the top contact for graphene

film and In-Ga alloy was pasted at the rear side of Ge as ohmic contact to the substrate. Photoelectrical characterization of the heterojunction device was carried out on a semiconductor parameter analyzer system (Keithley 4200-SCS, Tektronix) by using light sources with different wavelengths of 265, 780, 980, 1310, 1550 and 3043 nm. To detect the response speed, pulsed optical signals with varied frequencies were produced by driving a 980 nm laser diode with a function generator (SDG1032X, Siglent), and then the output photocurrent was recorded with an oscilloscope (DPO2012B, Tektronix). To perform the spectral response characterization, a Xe lamp (Gloria-X150A, Zolix Instruments) equipped with a monochromator (Omni-λ300, Zolix Instruments) was used to produce the monochromatic light with wavelength ranging from 200 to 2200 nm.

Theoretical calculations. Band structure calculations of the $PdSe_2$ film were performed using the density functional theory (DFT) with the projector augmented wave method[34] in the Vienna *ab initio* simulation package (VASP).[35] Perdew-Burke-Ernzerh of exchange-correlation potential functional within the generalized gradient approximation was employed.[36] The energy cut-off of 500 eV and a grid of 7×7×1 were used for the sample in the Brillouin zone. The converged thresholds of 10^{-5} eV and 0.01 eV/Å were used to optimize the hetero-multilayers for total energy and atom force, respectively. A vacuum interval of 2 nm was inserted to avoid artificial interactions between the neighboring layers.

Optical properties of the $PdSe_2$ film can be obtained by the dielectric function, which can be expressed as: $\varepsilon(\omega) = \varepsilon_1(\omega) + i\varepsilon_2(\omega)$. The imaginary part $\varepsilon_2(\omega)$ can be calculated from the momentum matrix elements between the occupied and unoccupied wave functions with the selection rules, and the real part $\varepsilon_1(\omega)$ can be evaluated from the imaginary part by Kramer-Kronig relationships:

$$\varepsilon_2(w) = \frac{4\pi^2 e^2}{m^2 w^2} \sum_{nn'} \int \left| P_{nn'}(k) \right|^2 \frac{dS_k}{\nabla w_{nn'}(k)} \tag{4}$$

$$\varepsilon_1(w) = 1 + \frac{2}{\pi} p \sum_{nn'} \int \frac{w' \varepsilon_2(w')}{w'^2 - w^2} dw' \tag{5}$$

where $P_{nn'}(k)$, $\omega_{nn'}(k)$, S_k and p represent the dipole matrix element, the energy difference between initial and final states, constant of a surface energy and the principal part of the integral, respectively. The optical absorption coefficient *a(ω)* can be further obtained by using the above parameters as follows:

$$\alpha(\omega) = \sqrt{2}\omega [\sqrt{\varepsilon_1^2(\omega) + \varepsilon_2^2(\omega)} - \varepsilon_1(\omega)]^{\frac{1}{2}} \tag{6}$$

FIGURES

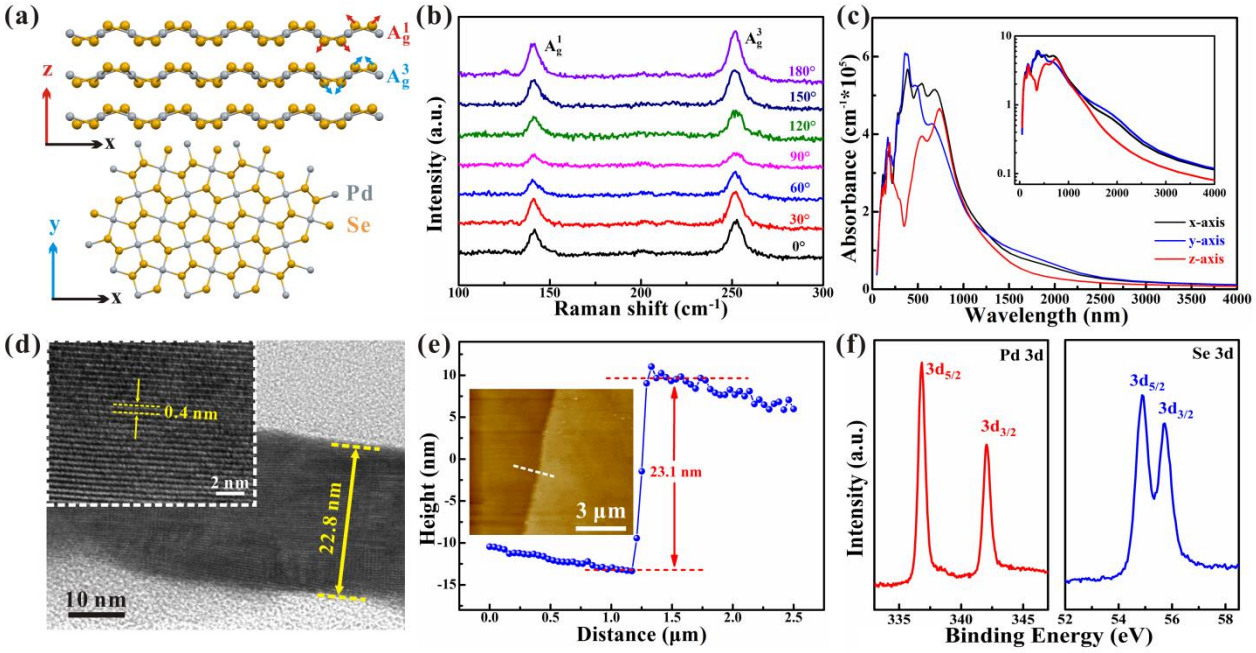

Figure 1. (a) Crystal structure of $PdSe_2$. (b) Polarization-dependent Raman spectra of $PdSe_2$ film. (c) Calculated optical absorbance of $PdSe_2$ with polarized light along different axis. (d) Cross-sectional TEM image and HRTEM (inset) of the $PdSe_2$ film. (e) AFM image and corresponding height profile of the $PdSe_2$ film. (f) XPS spectra of Pd 3d and Se 3d.

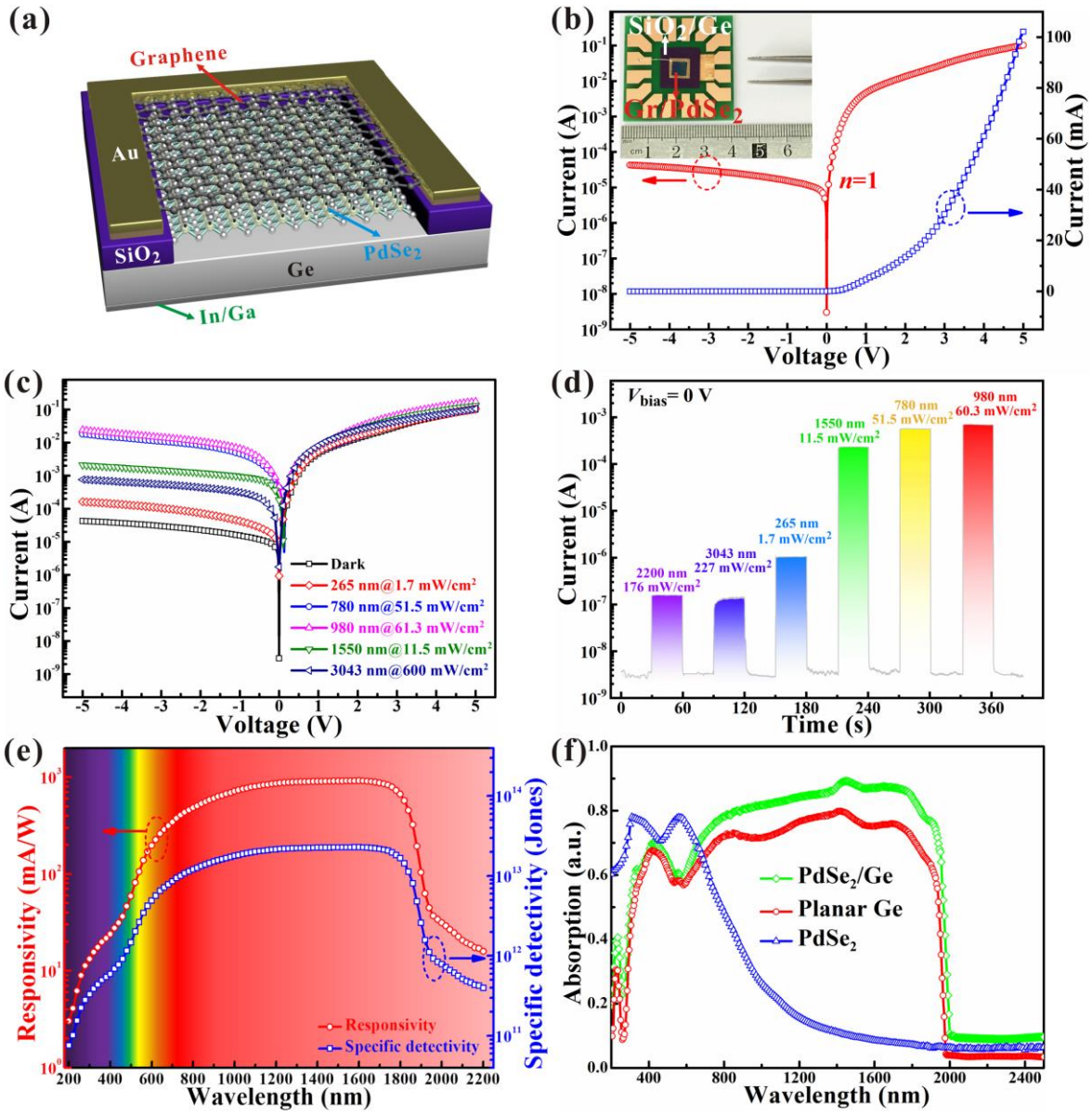

Figure 2. (a) Schematic diagram of the Gr/$PdSe_2$/Ge heterojunction device. (b) *I-V* curves of the heterojunction device in linear and logarithmic coordinates, respectively, in the dark. Inset shows a photograph of the heterojunction device. (c) *I-V* curves and (d) time-resolved photoresponse properties of the device under light illumination with different wavelengths. (e) Wavelength-dependent responsivity and specific detectivity of the Gr/$PdSe_2$/Ge heterojunction device. (f) Absorption spectra of the $PdSe_2$ film, Ge substrate and $PdSe_2$/Ge heterojunction.

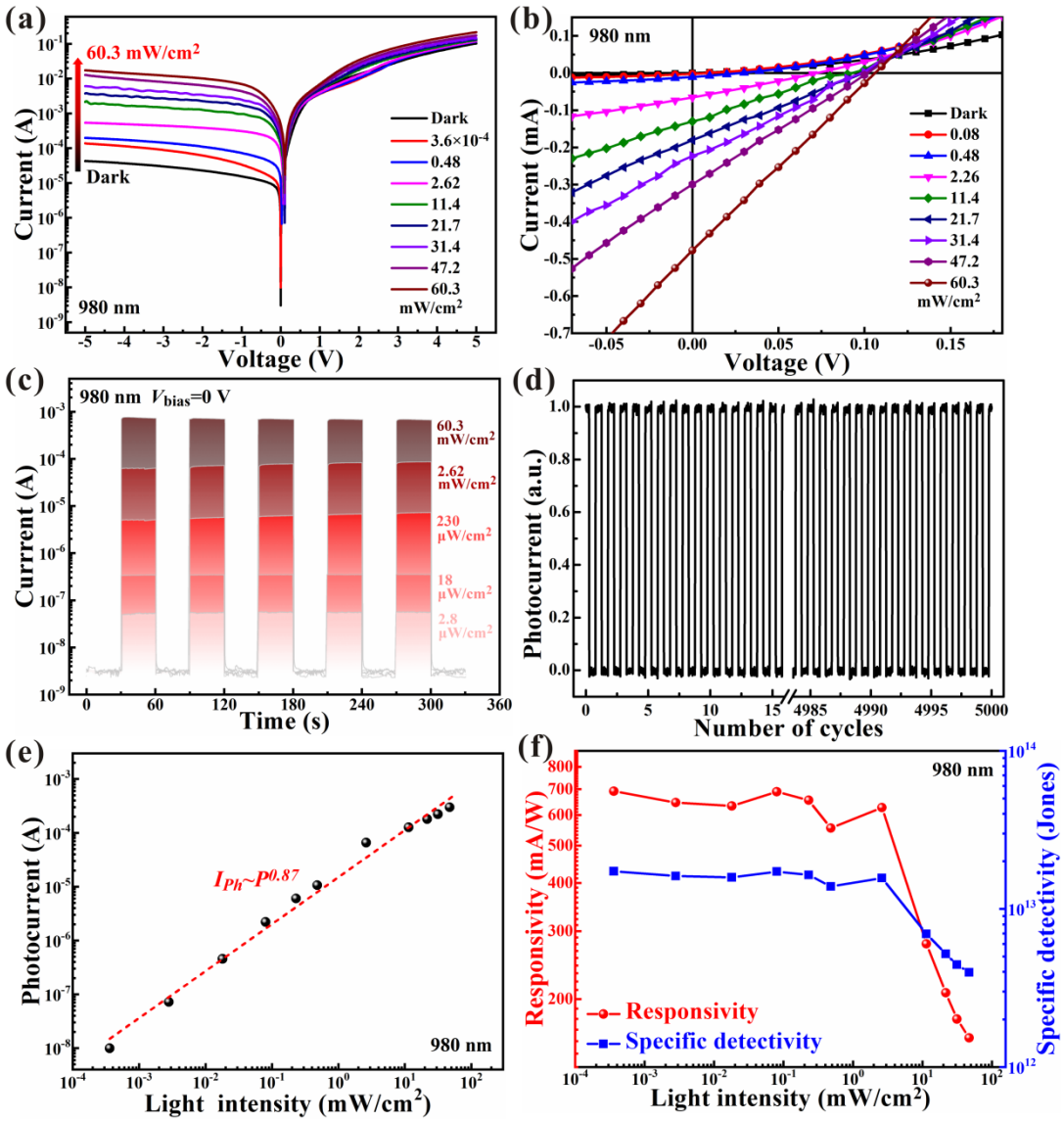

Figure 3. (a) *I-V* curves of the Gr/$PdSe_2$/Ge heterojunction device measured under light illumination of 980 nm with varied light intensities. (b) Enlarged *I-V* curves show the photovoltaic behavior of the heterojunction device. (c) Time-resolved photoresponse properties of the device under light illumination with different light intensities at 0 V. (d) Five thousand continuous response cycles of the device. (e) Photocurrent as a function of the light intensity in a double logarithmic coordinates. (f) Light intensity-dependent responsivity and specific detectivity of the Gr/$PdSe_2$/Ge heterojunction photodetector.

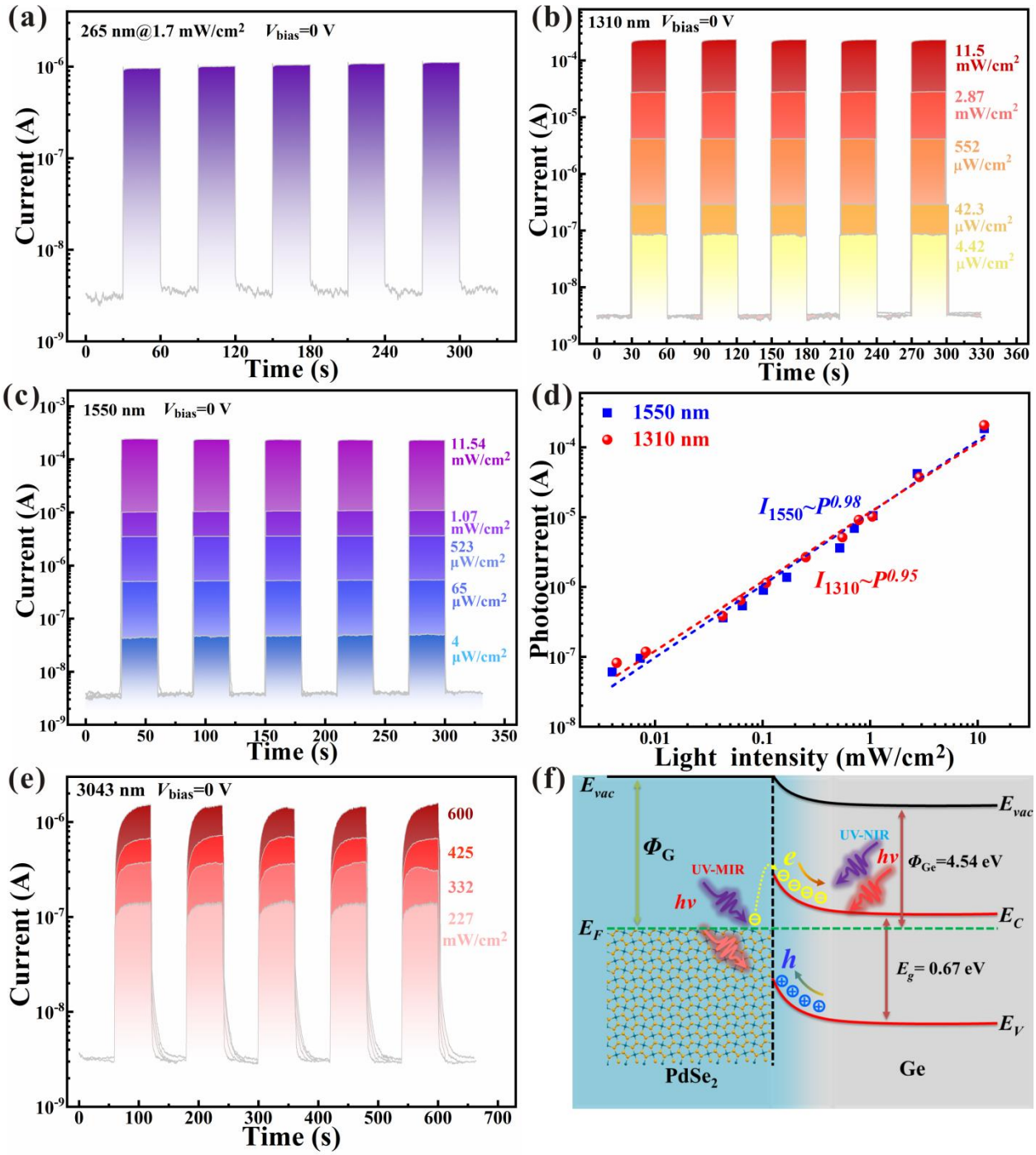

Figure 4. Time-resolved photoresponse of Gr/$PdSe_2$/Ge heterojunction photodetector to lights of (a) 265 nm, (b) 1310 nm, (c) 1550 nm, and (e) 3043 nm, respectively. (d) Photocurrents as a function of light intensity for 1310 and 1550 nm in a double logarithmic coordinates. (f) Energy band diagram of the Gr/$PdSe_2$/Ge heterojunction under light illumination.

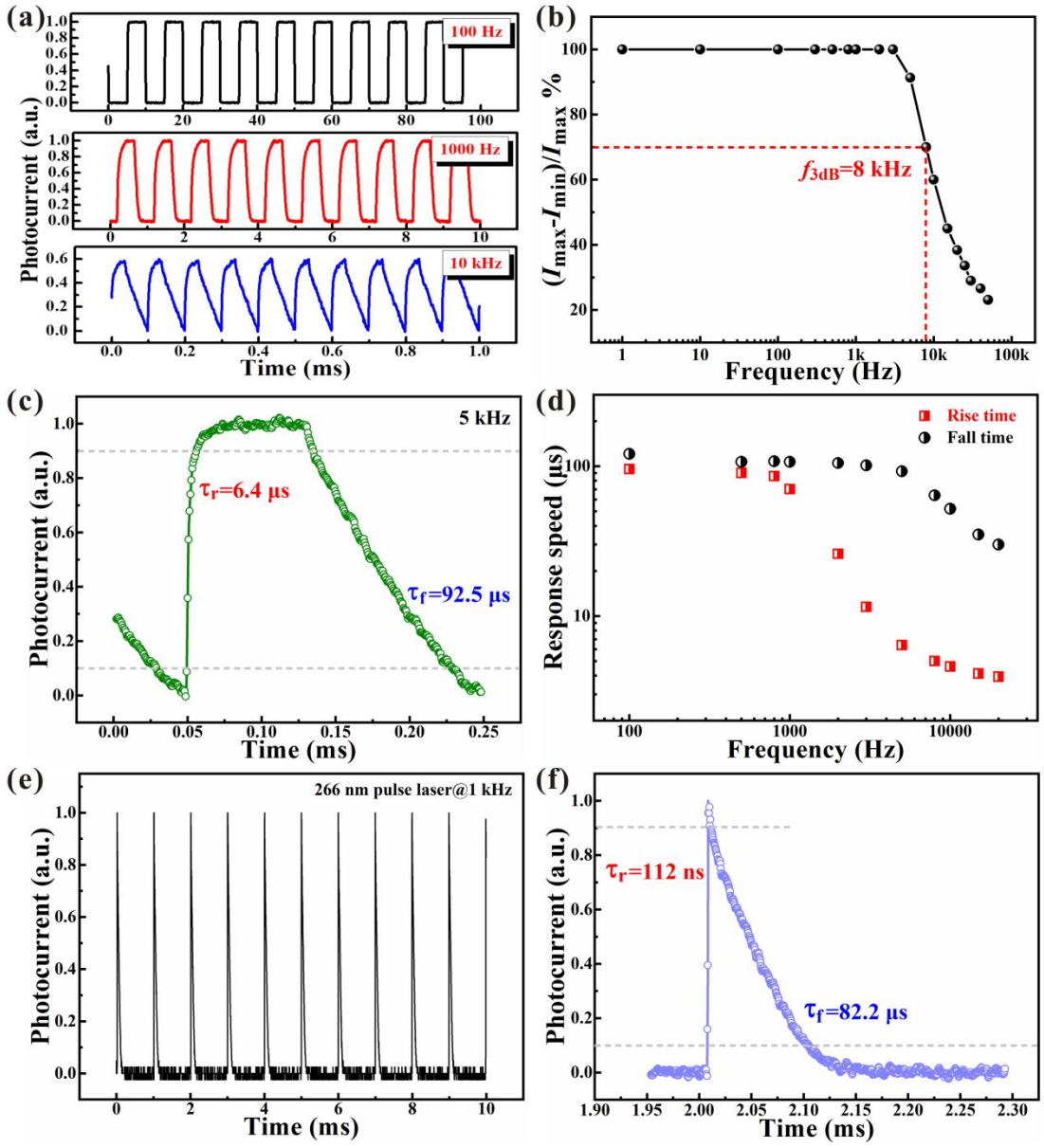

Figure 5. (a) Photoresponse properties of the Gr/$PdSe_2$/Ge heterojunction to pulsed light (980 nm) with different frequencies of 100 Hz, 1000 Hz, and10 kHz, respectively. (b) Relative balance [$(I_{max} - I_{min})/I_{max}$] as a function of switching frequency. (c) A single normalized response for estimating the response speeds at 5 kHz. (d) Response speeds at different switching frequency. (e) Photoresponse of the heterojunction to 266 nm pulsed laser at 1 kHz with a pulse width of 1 ns. (f) An enlarged response for evaluating response speeds.

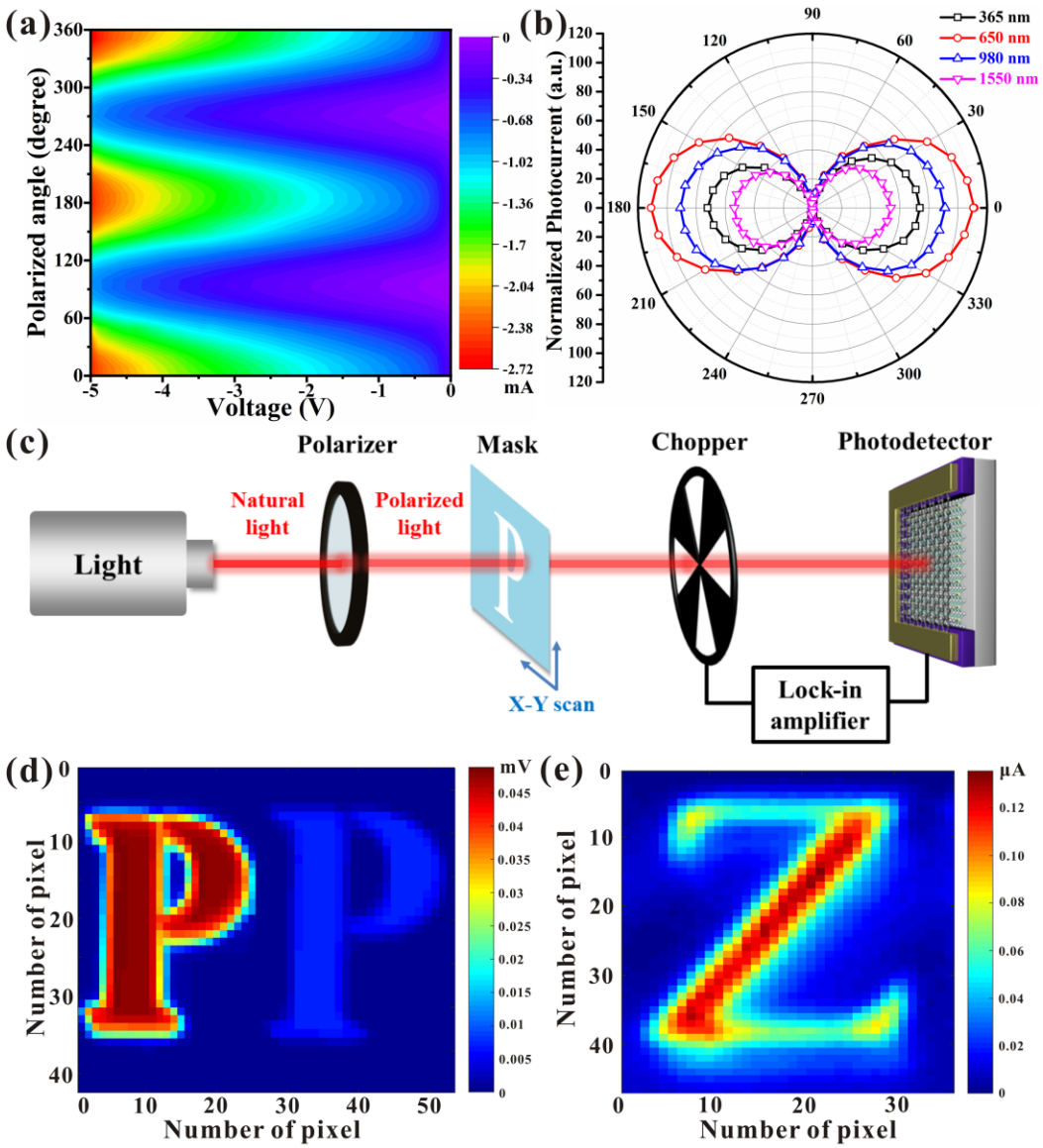

Figure 6. (a) Polarization-dependent current mapping under the light illumination of 650 nm at reverse bias from -5 V to 0 V. (b) Normalized photocurrent of the Gr/$PdSe_2$/Ge heterojunction as a function of the polarization angle at zero bias under polarized lights of 365 (40.5 mW/cm^2), 650 (52.6 mW/cm^2), 980 (60.3 mW/cm^2) and 1550 nm (11.5 mW/cm^2), respectively. (c) Schematic illustration of the measurement system for polarization-sensitive infrared imaging. (d) The imaging results of "P" letter under 780 nm with polarization angles of 0° (left) and 90° (right), respectively. (e) The MIR imaging pattern of "Z" letter under 3043 nm light.

Table 1. Comparison of the device performance of Gr/$PdSe_2$/Ge heterojunction photodetector with other reported 2D material-based photodetectors.

Device	λ (μm)	Self-powered	Polarization sensitivity	*R* (mA/W)	*D** (Jones)	Rise/fall time (μs)	Ref.
Gr/$PdSe_2$/Ge	0.2 – 3.04	Yes	112.2	691	1.73×10^{13}	6.4/92.5	This work
$PdSe_2$/MoS_2	0.45 – 10.6	Yes	/	185.6	8.21×10^{9}	65.3/62.4	[13]
$PtSe_2$/GaAs	0.25 – 1.2	Yes	/	262	2.52×10^{12}	5.5/6.5	[21]
Graphene/Ge	1.2 – 1.6	Yes	/	51.8	1.38×10^{10}	23/108	[15]
MoS_2/Ge	0.35 – 1.1	Yes	/	16.66	/	/	[37]
BP/WSe_2	0.4 – 1.55	No	~6	500	$\sim10^{10}$	800/800	[38]
GeS_2	0.25 – 0.4	No	2.1	/	/	/	[5]
BP/MoS_2	~1 – 3.8	Yes	~22	/	1.1×10^{10}	3.7/4	[11]

ASSOCIATED CONTENT

Supporting Information.

The Supporting Information is available free of charge on the ACS Publications website. The XRD pattern, digital image of a 2-inch $PdSe_2$ film. Raman spectra and Raman mapping image of the $PdSe_2$ film. Angle-resolved intensities of Raman peaks. AFM image and cross-sectional TEM image of the film. Photograph, optical microscope image and *I-V* curve of a transferred $PdSe_2$ film. Electrical contacts of $PdSe_2$ film and Ge substrate. Photovoltaic behavior, noise current and stability of the Gr/$PdSe_2$/Ge heterojuncion device. Air stability, theoretical bandgap and UPS result of the $PdSe_2$ film. Schematic diagram for the polarization sensitivity measurement. Polarization response of the $PdSe_2$ film. Digital photograph of the measurement system for imaging application. AFM image of the initial Pd film.

AUTHOR INFORMATION

Corresponding Author

*Longhui Zeng, E-mail: lhzeng.hfut@gmail.com

*Yuen Hong Tsang, E-mail: yuen.tsang@polyu.edu.hk

*Jiansheng Jie, E-mail: jsjie@suda.edu.cn

Author Contributions

The manuscript was written through contributions of all authors. All authors have given approval to the final version of the manuscript.

The authors declare no competing financial interest.

ACKNOWLEDGMENT

This work was financially supported by the National Natural Science Foundation of China (Nos. 51821002, 91833303, 61605174, 61774136, and 11604302), Research Grants Council of Hong Kong, China (Project Number: GRF 152109/16E and GRF 152093/18E PolyU B-Q65N), the Priority Academic Program Development of Jiangsu Higher Education Institutions (PAPD), the 111 Project, and Collaborative Innovation Center of Suzhou Nano Science and Technology (Nano-CIC).

REFERENCES

(1) Wang, J.; Gudiksen, M. S.; Duan, X.; Cui, Y.; Lieber, C. M. Highly Polarized Photoluminescence and Photodetection from Single Indium Phosphide Nanowires. *Science* **2001,** *293*, 1455-1457.

(2) Zhang, E.; Wang, P.; Li, Z.; Wang, H.; Song, C.; Huang, C.; Chen, Z. G.; Yang, L.; Zhang, K.; Lu, S.; Wang, W.; Liu, S.; Fang, H.; Zhou, X.; Yan, H.; Zou, J.; Wan, X.; Zhou, P.; Hu, W.; Xiu, F. Tunable Ambipolar Polarization-Sensitive Photodetectors Based on High-Anisotropy $ReSe_2$ Nanosheets. *ACS Nano* **2016,** *10*, 8067-8077.

(3) Oyedele, A. D.; Yang, S.; Liang, L.; Puretzky, A. A.; Wang, K.; Zhang, J.; Yu, P.; Pudasaini, P. R.; Ghosh, A. W.; Liu, Z.; Rouleau, C. M.; Sumpter, B. G.; Chisholm, M. F.; Zhou, W.; Rack, P. D.; Geohegan, D. B.; Xiao, K. $PdSe_2$: Pentagonal Two-Dimensional Layers with High Air Stability for Electronics. *J. Am. Chem. Soc.* **2017,** *139*, 14090-14097.

(4) Yuan, H.; Liu, X.; Afshinmanesh, F.; Li, W.; Xu, G.; Sun, J.; Lian, B.; Curto, A. G.; Ye, G.; Hikita, Y.; Shen, Z.; Zhang, S. C.; Chen, X.; Brongersma, M.; Hwang, H. Y.; Cui, Y. Polarization-Sensitive Broadband Photodetector Using a Black Phosphorus Vertical *p-n* Junction. *Nat. Nanotechnol.* **2015,** *10*, 707-713.

(5) Yang, Y.; Liu, S.-C.; Wang, X.; Li, Z.; Zhang, Y.; Zhang, G.; Xue, D.-J.; Hu, J.-S. Polarization-Sensitive Ultraviolet Photodetection of Anisotropic 2D GeS_2. *Adv. Funct. Mater.* **2019,** *29*, 1900411.

(6) Tao, L.; Cinquanta, E.; Chiappe, D.; Grazianetti, C.; Fanciulli, M.; Dubey, M.; Molle, A.; Akinwande, D. Silicene Field-Effect Transistors Operating at Room Temperature. *Nat. Nanotechnol.* **2015,** *10*, 227.

(7) Li, L.; Lu, S.-z.; Pan, J.; Qin, Z.; Wang, Y.-q.; Wang, Y.; Cao, G.-y.; Du, S.; Gao, H.-J. Buckled Germanene Formation on Pt(111). *Adv. Mater.* **2014,** *26*, 4820-4824.

(8) Chu, F.; Chen, M.; Wang, Y.; Xie, Y.; Liu, B.; Yang, Y.; An, X.; Zhang, Y. A Highly Polarization Sensitive Antimonene Photodetector with a Broadband Photoresponse and Strong Anisotropy. *J. Mater. Chem. C* **2018,** *6*, 2509-2514.

(9) Quhe, R.; Fei, R.; Liu, Q.; Zheng, J.; Li, H.; Xu, C.; Ni, Z.; Wang, Y.; Yu, D.; Gao, Z.; Lu, J. Tunable and Sizable Band Gap in Silicene by Surface Adsorption. *Sci. Rep.* **2012,** *2*, 853.

(10) Venuthurumilli, P. K.; Ye, P. D.; Xu, X. Plasmonic Resonance Enhanced Polarization-Sensitive Photodetection by Black Phosphorus in Near Infrared. *ACS Nano* **2018,** *12*, 4861-4867.

(11) Bullock, J.; Amani, M.; Cho, J.; Chen, Y.-Z.; Ahn, G. H.; Adinolfi, V.; Shrestha, V. R.; Gao, Y.; Crozier, K. B.; Chueh, Y.-L.; Javey, A. Polarization-Resolved Black Phosphorus/Molybdenum Disulfide Mid-Wave Infrared Photodiodes with High Detectivity at Room Temperature. *Nat. Photonics* **2018,** *12*, 601-607.

(12) Zeng, L.-H.; Wu, D.; Lin, S.-H.; Xie, C.; Yuan, H.-Y.; Lu, W.; Lau, S. P.; Chai, Y.; Luo, L.-B.; Li, Z.-J.; Tsang, Y. H. Controlled Synthesis of 2D Palladium Diselenide for Sensitive Photodetector Applications. *Adv. Funct. Mater.* **2019,** *29*, 1806878.

(13) Long, M.; Wang, Y.; Wang, P.; Zhou, X.; Xia, H.; Luo, C.; Huang, S.; Zhang, G.; Yan, H.;

Fan, Z.; Wu, X.; Chen, X.; Lu, W.; Hu, W. Palladium Diselenide Long-Wavelength Infrared Photodetector with High Sensitivity and Stability. *ACS Nano* **2019,** *13*, 2511-2519.

(14) Chow, W. L.; Yu, P.; Liu, F.; Hong, J.; Wang, X.; Zeng, Q.; Hsu, C. H.; Zhu, C.; Zhou, J.; Wang, X.; Xia, J.; Yan, J.; Chen, Y.; Wu, D.; Yu, T.; Shen, Z.; Lin, H.; Jin, C.; Tay, B. K.; Liu, Z. High Mobility 2D Palladium Diselenide Field-Effect Transistors with Tunable Ambipolar Characteristics. *Adv. Mater.* **2017,** *29*, 1602969.

(15) Zeng, L.-H.; Wang, M.-Z.; Hu, H.; Nie, B.; Yu, Y.-Q.; Wu, C.-Y.; Wang, L.; Hu, J.-G.; Xie, C.; Liang, F.-X.; Luo, L.-B. Monolayer Graphene/Germanium Schottky Junction As High-Performance Self-Driven Infrared Light Photodetector. *ACS Appl. Mater. Interfaces* **2013,** *5*, 9362-9366.

(16) Yim, C.; Lee, K.; McEvoy, N.; O'Brien, M.; Riazimehr, S.; Berner, N. C.; Cullen, C. P.; Kotakoski, J.; Meyer, J. C.; Lemme, M. C.; Duesberg, G. S. High-Performance Hybrid Electronic Devices from Layered $PtSe_2$ Films Grown at Low Temperature. *ACS Nano* **2016,** *10*, 9550-9558.

(17) Sah, C.; Noyce, R. N.; Shockley, W. Carrier Generation and Recombination in *P-N* Junctions and *P-N* Junction Characteristics. *Proc. IRE* **1957,** *45*, 1228-1243.

(18) Gong, X.; Tong, M.; Xia, Y.; Cai, W.; Moon, J. S.; Cao, Y.; Yu, G.; Shieh, C.-L.; Nilsson, B.; Heeger, A. J. High-Detectivity Polymer Photodetectors with Spectral Response from 300 nm to 1450 nm. *Science* **2009,** *325*, 1665-1667.

(19) Xie, C.; Mak, C.; Tao, X.; Yan, F. Photodetectors Based on Two-Dimensional Layered Materials Beyond Graphene. *Adv. Funct. Mater.* **2017,** *27*, 1603886.

(20) Kung, S.-C.; van der Veer, W. E.; Yang, F.; Donavan, K. C.; Penner, R. M. 20 μs Photocurrent Response from Lithographically Patterned Nanocrystalline Cadmium Selenide

Nanowires. *Nano Lett.* **2010,** *10*, 1481-1485.

(21) Zeng, L.-H.; Lin, S.-H.; Li, Z.-J.; Zhang, Z.-X.; Zhang, T.-F.; Xie, C.; Mak, C.-H.; Chai, Y.; Lau, S. P.; Luo, L.-B.; Tsang, Y. H. Fast, Self-Driven, Air-Stable, and Broadband Photodetector Based on Vertically Aligned $PtSe_2$/GaAs Heterojunction. *Adv. Funct. Mater.* **2018,** *28*, 1705970.

(22) Yu, X.; Yu, P.; Wu, D.; Singh, B.; Zeng, Q.; Lin, H.; Zhou, W.; Lin, J.; Suenaga, K.; Liu, Z.; Wang, Q. J. Atomically Thin Noble Metal Dichalcogenide: A Broadband Mid-Infrared Semiconductor. *Nat. Commun.* **2018,** *9*, 1545.

(23) Tang, Y.; Wang, Z.; Wang, P.; Wu, F.; Wang, Y.; Chen, Y.; Wang, H.; Peng, M.; Shan, C.; Zhu, Z.; Qin, S.; Hu, W. WSe_2 Photovoltaic Device Based on Intramolecular *p-n* Junction. *Small* **2019,** *15*, e1805545.

(24) Wang, P.; Liu, S.; Luo, W.; Fang, H.; Gong, F.; Guo, N.; Chen, Z. G.; Zou, J.; Huang, Y.; Zhou, X.; Wang, J.; Chen, X.; Lu, W.; Xiu, F.; Hu, W. Arrayed Van Der Waals Broadband Detectors for Dual-Band Detection. *Adv. Mater.* **2017,** *29*, 1604439.

(25) Wu, E.; Wu, D.; Jia, C.; Wang, Y.; Yuan, H.; Zeng, L.; Xu, T.; Shi, Z.; Tian, Y.; Li, X. *In Situ* Fabrication of 2D WS_2/Si Type-II Heterojunction for Self-Powered Broadband Photodetector with Response up to Mid-Infrared. *ACS Photonics* **2019,** *6*, 565-572.

(26) Xiao, P.; Mao, J.; Ding, K.; Luo, W.; Hu, W.; Zhang, X.; Zhang, X.; Jie, J. Solution-Processed 3D RGO-MoS_2/Pyramid Si Heterojunction for Ultrahigh Detectivity and Ultra-Broadband Photodetection. *Adv. Mater.* **2018,** *30*, 1801729.

(27) Wu, D.; Wang, Y.; Zeng, L.; Jia, C.; Wu, E.; Xu, T.; Shi, Z.; Tian, Y.; Li, X.; Tsang, Y. H. Design of 2D Layered $PtSe_2$ Heterojunction for the High-Performance, Room-Temperature, Broadband, Infrared Photodetector. *ACS Photonics* **2018,** *5*, 3820-3827.

(28) Mao, J.; Yu, Y.; Wang, L.; Zhang, X.; Wang, Y.; Shao, Z.; Jie, J. Ultrafast, Broadband

Photodetector Based on $MoSe_2$/Silicon Heterojunction with Vertically Standing Layered Structure Using Graphene as Transparent Electrode. *Adv. Sci.* **2016,** *3*, 1600018.

(29) Yang, Y.; Liu, S. C.; Yang, W.; Li, Z.; Wang, Y.; Wang, X.; Zhang, S.; Zhang, Y.; Long, M.; Zhang, G.; Xue, D. J.; Hu, J. S.; Wan, L. J. Air-Stable In-Plane Anisotropic $GeSe_2$ for Highly Polarization-Sensitive Photodetection in Short Wave Region. *J. Am. Chem. Soc.* **2018,** *140*, 4150-4156.

(30) Gao, L.; Zeng, K.; Guo, J.; Ge, C.; Du, J.; Zhao, Y.; Chen, C.; Deng, H.; He, Y.; Song, H.; Niu, G.; Tang, J. Passivated Single-Crystalline $CH_3NH_3PbI_3$ Nanowire Photodetector with High Detectivity and Polarization Sensitivity. *Nano Lett.* **2016,** *16*, 7446-7454.

(31) Mukherjee, S.; Das, K.; Das, S.; Ray, S. K. Highly Responsive, Polarization Sensitive, Self-Biased Single GeO_2-Ge Nanowire Device for Broadband and Low Power Photodetectors. *ACS Photonics* **2018,** *5*, 4170-4178.

(32) Liang, Q.; Wang, Q.; Zhang, Q.; Wei, J.; Lim, S. X.; Zhu, R.; Hu, J.; Wei, W.; Lee, C.; Sow, C.; Zhang, W.; Wee, A. T. S. High-Performance, Room Temperature, Ultra-Broadband Photodetectors Based on Air-Stable $PdSe_2$. *Adv. Mater.* **2019**, *31*, e1807609.

(33) Zeng, L.; Lin, S.; Lou, Z.; Yuan, H.; Long, H.; Li, Y.; Lu, W.; Lau, S. P.; Wu, D.; Tsang, Y. H. Ultrafast and Sensitive Photodetector Based on A $PtSe_2$/Silicon Nanowire Array Heterojunction with A Multiband Spectral Response from 200 to 1550 nm. *NPG Asia Mater.* **2018,** *10*, 352-362.

(34) Blöchl, P. E. Projector Augmented-Wave Method. *Phys. Rev. B* **1994,** *50*, 17953-17979.

(35) Kresse, G.; Furthmüller, J. Efficient Iterative Schemes for *Ab initio* Total-Energy Calculations Using A Plane-Wave Basis Set. *Phys. Rev. B* **1996,** *54*, 11169-11186.

(36) Perdew, J. P.; Burke, K.; Ernzerhof, M. Generalized Gradient Approximation Made Simple.

Phys. Rev. Lett. **1996,** *77*, 3865-3868.

(37) Mahyavanshi, R. D.; Kalita, G.; Ranade, A.; Desai, P.; Kondo, M.; Dewa, T.; Tanemura, M. Photovoltaic Action With Broadband Photoresponsivity in Germanium-MoS_2 Ultrathin Heterojunction. *IEEE Trans. Electron Devices* **2018,** *65*, 4434-4440.

(38) Ye, L.; Wang, P.; Luo, W.; Gong, F.; Liao, L.; Liu, T.; Tong, L.; Zang, J.; Xu, J.; Hu, W. Highly Polarization Sensitive Infrared Photodetector Based on Black Phosphorus-on-WSe_2 Photogate Vertical Heterostructure. *Nano Energy* **2017,** *37*, 53-60.

For Table of Contents Only